Check for updates

JGR Atmospheres

RESEARCH ARTICLE
10.1029/2026JD047362

Terrain-Induced Contrasts in the Diurnal Variations of Low-Level Jets Over the Middle Reaches of the Yangtze River During the 2010 Mei-yu Field Campaign

Wen Zhou[1], Yu Du[2], Yang Hu[1], Xiaofang Wang[1], and Chunguang Cui[1]

[1]Heavy Rainfall Research Center of China/China Meteorological Administration Basin Heavy Rainfall Key Laboratory/Hubei Key Laboratory for Heavy Rain Monitoring and Warning Research, Institute of Heavy Rain, China Meteorological Administration, Wuhan, China, [2]Southern Marine Science and Engineering Guangdong Laboratory (Zhuhai), School of Atmospheric Sciences, Sun Yat-sen University, Zhuhai, China

Abstract The diurnal cycle of low-level jets (LLJs) plays a crucial role in severe convective weather during the Mei-yu season over the middle reaches of the Yangtze River (MRYR). However, previous studies have focused on individual sites or large-scale climatic contrasts, leaving sub-regional variations in LLJ diurnal behaviors and their governing mechanisms insufficiently understood. Using intensive radiosonde observations from three topographically distinct sites during the 2010 Mei-yu field campaign, combined with ERA5 reanalysis, we partially address this knowledge gap. Results show that (a) LLJ occurrence exhibits a single peak between 1.5 and 2.5 km AGL in terrain-affected regions, dominated by synoptic-system-related LLJs (SLLJs) with higher core altitudes, whereas a double-peak structure appears over plains, where both boundary-layer jets (BLJs) and SLLJs frequently occur. (b) In terrain-affected regions, SLLJ frequency and intensity peak at night, governed by nocturnal inertial oscillation with deeper boundary layers. In contrast, over plains, SLLJs peak during the daytime due to northward advancement of the Western Pacific Subtropical High (WPSH). Nocturnal BLJs over plains are influenced by both inertial oscillation and WPSH westward extension. (c) In terrain-affected regions, SLLJ core heights descend from 20:00 to 02:00 LST and then ascend, modulated by the boundary layer via capping inversions that inhibit vertical momentum transfer and maintain a strong momentum layer aloft. Over plains, this descending phase persists until 08:00 LST, associated with intensifications of Mei-yu fronts at 800 hPa. Derived from a single Mei-yu period, results may not be representative of multi-year climatological conditions. These findings advance dynamical understanding of terrain-induced contrasts in LLJs over the MRYR and provide a benchmark for evaluating numerical simulations.

Plain Language Summary This study used intensive radiosonde observations from three distinct terrain types (mountains, a transition zone, and plains) during the 2010 Mei-yu period, combined with ERA5 reanalysis data, to examine LLJ differences. Results show that the vertical structure and diurnal cycle of LLJs differ greatly by terrain during the 2010 Mei-yu field campaign: in mountainous areas, jets above the boundary layer dominate and show a single nighttime peak driven by inertial oscillations, while over plains, jets occur frequently both below and above the boundary layer, with two daily peaks shaped by large-scale weather systems and inertial oscillations. In addition, the jet-core height of SLLJs experiences an initial downward trend followed by a subsequent upward trend, with a more prolonged downward phase over the plains. These results advance our understanding of terrain effects on LLJs and provide a useful benchmark for numerical simulations during Mei-yu season. Note that these findings are derived using observations from only one Mei-yu field campaign and may not reflect climatological features across multiple years.

Key Points:

- From 2010 observations, vertical distributions of low-level jets (LLJs) show double-peak (single-peak) patterns over plains (terrain-affected regions)
- Distinct diurnal shifting patterns of jet core height in terrain-affected regions and plains are identified during the 2010 Mei-yu period
- Inertial oscillation governs diurnal variations of synoptic-system-related LLJs in the terrain-affected regions in the 2010 Mei-yu season

Supporting Information:

Supporting Information may be found in the online version of this article.

Correspondence to:

Y. Du,
duyu7@mail.sysu.edu.cn

Citation:

Zhou, W., Du, Y., Hu, Y., Wang, X., & Cui, C. (2026). Terrain-induced contrasts in the diurnal variations of low-level jets over the middle reaches of the Yangtze River during the 2010 Mei-yu field campaign. *Journal of Geophysical Research: Atmospheres*, *131*, e2026JD047362. https://doi.org/10.1029/2026JD047362

Received 29 APR 2026
Accepted 12 SEP 2026

© 2026 The Author(s). Journal of Geophysical Research: Atmospheres published by Wiley Periodicals LLC on behalf of American Geophysical Union. This is an open access article under the terms of the Creative Commons Attribution License, which permits use, distribution and reproduction in any medium, provided the original work is properly cited.

1. Introduction

Low-level jets (LLJs) are intense wind streams in the lower troposphere (Bonner, 1968; Marengo et al., 2004; Whiteman et al., 1997), and they are often classified into two types: (a) boundary layer jets (BLJs), which occur within the boundary layer; and (b) synoptic-system-related LLJs (SLLJs), which occur in the layers above the boundary layer (Du & Chen, 2019). Both types are typically characterized by a distinct "nose-shaped" wind speed profile (Y. L. Chen et al., 1994; H. Liu et al., 2014; M. Zhang & Meng, 2019). Owing to their strong wind speeds and pronounced vertical shear, LLJs are widely recognized as critical dynamical drivers of severe convective weather (G. T. J. Chen et al., 2005; Du et al., 2012; Li et al., 2024; Xue et al., 2018).

21698996, 2026, 18, Downloaded from https://agupubs.onlinelibrary.wiley.com/doi/10.1029/2026JD047362, Wiley Online Library on [04/11/2026]. See the Terms and Conditions (https://onlinelibrary.wiley.com/terms-and-conditions) on Wiley Online Library for rules of use; OA articles are governed by the applicable Creative Commons License

In particular, the diurnal variations of LLJs play a crucial role in regulating the evolution of convective systems, as their diurnal behaviors directly regulate the supply of moisture and the location of low-level convergence (Du & Yi, 2025; Du et al., 2022; X. Liu et al., 2020; Shen & Du, 2023; C. Zhou et al., 2026). Understanding the diurnal cycle of LLJs is therefore essential for improving understanding and forecasting of severe convective events, particularly during the Mei-yu season when such events are most active (C. Cui et al., 2023; Hu et al., 2021).

LLJ characteristics exhibit considerable regional diversity, particularly in terms of their vertical structure and core heights. Early observational work documented the existence of strong LLJs across different regions, including the cross-equatorial jets over the western Indian Ocean, which typically develop near 1–1.5 km above ground level (AGL; Findlater, 1977). Over the North American Great Plains, LLJs typically occur below 1,000 m AGL (Farquharson, 1939; Means, 1952). A finding later refined by high-resolution observations over the mid-western United States, where LLJs are most frequently observed at 300–500 m AGL (Vanderwende et al., 2015). Over South America, the vertical structure of LLJs is strongly modulated by topography. At the upstream Andean foothill site of Santa Cruz (Bolivia), the jet core is centered at 1,000–1,500 m AGL, while at the downstream plain site of Mariscal (Paraguay), the jet core is significantly lower, typically occurring at 500–1,000 m AGL (Montini et al., 2019). In East Asia, by contrast, LLJs show more complex vertical structures. For example, observations around Okinawa reveal two frequent LLJ heights near 500–700 m and 1,100–1,300 m AGL (Pham et al., 2008). Further west, over the lower reaches of the Yangtze River, these core heights are found at higher altitudes, near 800 and 2,200 m (Du et al., 2012; W. Wei et al., 2014).

Within China, systematic differences in LLJ characteristics also exist among major climatic zones. Comparisons between western and eastern China indicate that BLJs dominate in western China, whereas both BLJs and SLLJs are prevalent in South China (Du & Chen, 2019; Du et al., 2014; Zheng et al., 2026). Zheng et al. (2026) further suggested that BLJs frequently form in mountainous and coastal regions. Significant contrasts are also found between north China and south China (Miao et al., 2018; W. Wei et al., 2014; Yan et al., 2021). For instance, LLJs in North China exhibit more pronounced diurnal variability, typically peaking at night (Miao et al., 2018). Intriguingly, even within the relatively uniform Mei-Yu monsoonal regime along the Yangtze River, notable contrasts exist between its lower and middle reaches: BLJs dominate in the Middle Reaches of the Yangtze River (MRYR), while SLLJs prevail in the lower reaches (C. Cui et al., 2023; Du et al., 2012; W. Wei et al., 2013). This large-scale heterogeneity indicates that LLJ characteristics are fundamentally shaped by regional factors such as terrain, land-sea contrast, and synoptic regimes (Zheng et al., 2026; C. Zhou et al., 2026). However, most previous studies have focused on large-scale climatic contrasts (Du et al., 2014; W. Wei et al., 2014; Zheng et al., 2026), leaving sub-regional variations in LLJ diurnal behaviors and their underlying mechanisms inadequately understood. Additionally, limited by the scarcity of in situ vertical observations, previous studies have mainly examined diurnal variations in LLJ frequency and intensity (Du & Chen, 2019; Zheng et al., 2026), whereas the diurnal variations of their fine-scale vertical structure received much less attention.

To explain regional differences in LLJ characteristics, various formation mechanisms have been proposed. The nocturnal intensification of BLJs is classically explained by inertial oscillations following the decay of turbulent mixing after sunset (Blackadar, 1957; Du & Rotunno, 2014). Additionally, thermal forcing over sloping terrain, such as mountain-plain solenoids, can also modulate low-level winds (Holton, 1967; Shu et al., 2024). In contrast, SLLJs are generally considered to be predominantly governed by synoptic-scale weather systems, such as fronts, southwest vortices and northeast cold vortices, which often leads to weaker diurnal variability in many regions (Du et al., 2012, 2014). Nevertheless, this assumption that SLLJs are largely independent of boundary-layer processes may not hold in regions with complex topography, where the boundary layer development can be more vigorous and heterogeneous (Tan et al., 2025). Yet, the degree to which terrain-modulated boundary-layer processes can influence SLLJs, potentially modifying their intensity, vertical structure, and diurnal evolution, remains poorly understood.

These unresolved knowledge gaps motivate the present investigation. We focus on the MRYR during the Mei-yu season, a region distinguished by a relatively coherent synoptic environment but pronounced topographic heterogeneity (Q. Wei et al., 2024). Utilizing synchronous intensive radiosonde observations from the 2010 Mei-yu field campaign alongside ERA5 reanalysis data, this study aims to achieve two primary objectives: (a) to systematically document sub-regional differences in LLJ characteristics (including occurrence frequency, jet core height, jet intensity, and diurnal evolution) among three distinct terrain regimes (mountain, mountain-plain transition, plain) across the MRYR; and (b) to quantitatively diagnose the mechanisms governing the diurnal

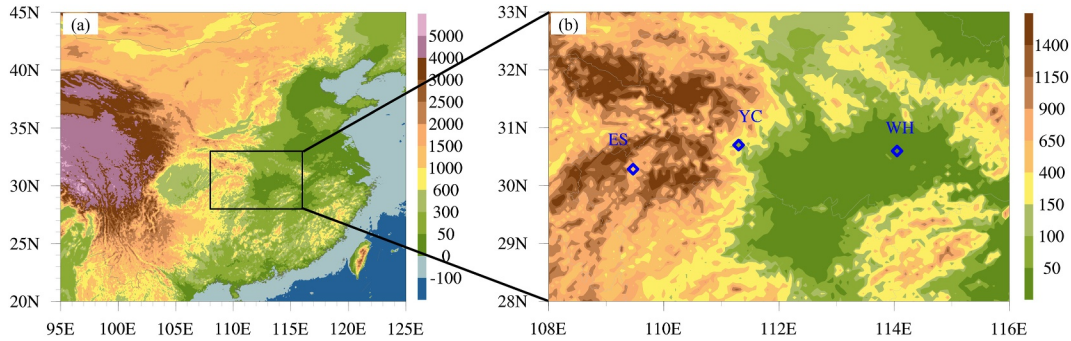


Figure 1. (a) Spatial distribution of topography (shading, units: m) across China. The black box indicates the study zone. (b) Topography (shading, units: m) across the MRYR. Blue markers, from west to east, represent the locations of intensive radiosonde observation sites at Enshi (ES, mountain region), Yichang (YC, mountain-plain region), and Wuhan (WH, plain region).

variability of LLJs (including jet core height, jet frequency and intensity) under different terrain conditions. Our analysis relies on observations from the 2010 Mei-yu season only. Although this observation period captures typical synoptic environments, the representativeness of the derived diurnal-variation results for long-term climatology remains limited.

The remainder of this paper is organized as follows: Section 2 describes the data and methodology. Section 3 presents the results, including observed sub-regional differences in LLJ characteristics and the associated dynamical mechanisms. Finally, conclusions and discussions are given in Section 4.

2. Data and Method

2.1. Observation Campaign and Data

This study utilized a unique transect of intensive radiosonde observations across the MRYR during the 2010 Mei-yu field campaign from 16 June to 30 July. Three sites were strategically deployed the main topographic gradient to represent distinct topographic regimes: Enshi (ES; 30.28°N, 109.47°E; 458 m) in the western complex mountainous region, Yichang (YC, 30.70°N, 111.30°E; 134 m) in the critical mountain-plain transition region, and Wuhan (WH, 30.60°N, 114.05°E; 24 m) in the eastern plain region (Figure 1). Soundings were launched at 3-hr intervals, providing a high vertical resolution of approximately 30 m to resolve the detailed diurnal evolution and vertical structure of LLJs. All radiosonde observations are obtained from the 2010 Mei-yu field campaign. Hence conclusions drawn from these data cannot be directly generalized to multi-year mean states.

A rigorous three-step quality control was applied to the raw radiosonde data to ensure reliability. First, a vertical range check retained only profiles with valid wind observations up to at least 4,000 m AGL. Second, abnormal profiles were removed by identifying wind speed outliers at individual levels within the 60–4,000 m AGL layer using the robust biweight method (Lanzante, 1996); any profile where the combined proportion of outlier levels and missing data exceeded 40% of the vertical range was discarded, following established practices (C. Cui et al., 2023; W. Wei et al., 2014). Third, any remaining missing or outlier data points within retained profiles were filled via linear interpolation. The final quality-controlled data set comprises 361, 360, and 348 valid profiles for ES, YC, and WH, respectively, forming a robust foundation for statistical analysis.

2.2. Reanalysis Data and Validation

To complement the point observations and facilitate a spatially consistent diagnostic analysis, this study employed the hourly 0.25° × 0.25° ERA5 reanalysis data (Hersbach et al., 2020). Before its diagnostic application, a validation was conducted to assess the fidelity of ERA5 in representing LLJ characteristics over the MRYR against the radiosonde observations. As will be detailed in Section 3.1, the reanalysis demonstrates credible skill in capturing the key statistical attributes and diurnal evolution of LLJs in this region, thereby supporting its use for subsequent mechanistic investigation.

21698996, 2026, 18, Downloaded from https://agupubs.onlinelibrary.wiley.com/doi/10.1029/2026JD047362, Wiley Online Library on [04/11/2026]. See the Terms and Conditions (https://onlinelibrary.wiley.com/terms-and-conditions) on Wiley Online Library for rules of use; OA articles are governed by the applicable Creative Commons License

21698996, 2026, 18, Downloaded from https://agupubs.onlinelibrary.wiley.com/doi/10.1029/2026JD047362, Wiley Online Library on [04/11/2026]. See the Terms and Conditions (https://onlinelibrary.wiley.com/terms-and-conditions) on Wiley Online Library for rules of use; OA articles are governed by the applicable Creative Commons License

2.3. Methodologies

LLJ identification and classification were performed using an objective algorithm following C. Cui et al. (2023). A wind profile was classified as containing an LLJ if it met two criteria: (a) a wind speed maximum exceeding 8.0 m s^{-1} within the 60–4,000 m AGL, and (b) a decrease in wind speed of at least 2.5 m s^{-1} from that maximum to any minimum above that height and below 4,000 m AGL, or to the 4,000 m level itself if no distinct minimum exists above that height. For all cases, the height and direction of the LLJ are assigned as the altitude and wind direction at the identified wind speed maximum. Based on the core height of the wind speed maximum, LLJs were further categorized: those with heights below 1.5 km AGL were defined as BLJs, while those with a core at or above 1.5 km AGL were termed SLLJs (C. Cui et al., 2023). Profiles exhibiting both a BLJ and an SLLJ were classified as double low-level jets (DLLJs).

The Planetary Boundary Layer Height (PBLH) was diagnosed as the height of the maximum potential temperature gradient within 3 km AGL, a widely accepted method in boundary layer studies (S. Liu & Liang, 2010; Tan et al., 2025). The potential temperature gradient was calculated using the central difference method (Stull, 1988), shown as Equation 2.

$$\theta = T\left(\frac{1000}{p}\right)^{0.286} \tag{1}$$

$$Gra_{\theta} = \frac{\partial \theta}{\partial z} \tag{2}$$

where T and p represent temperature and pressure, θ and Gra_{θ} indicate potential temperature and corresponding gradient, z represents height in AGL.

The diurnal cycle of LLJ occurrence frequency was quantified via harmonic analysis (Bell & Reid, 1993). The observed hourly frequency rate $F(t)$ was fitted to a Fourier series, shown as Equation 3, where $\omega = 2\pi(24\ \mathrm{hr})^{-1}$, and $t = 2,5,8,\ldots, 23$ hr. The coefficients a and b were derived via linear regression against the observed hourly frequency rates.

$$F(t) \approx f_0 + a \cdot \cos(\omega t) + b \cdot \sin(\omega t) \tag{3}$$

A momentum budget analysis was conducted to quantify the contributions of different physical processes to LLJ evolution (Du et al., 2022; X. Zhang et al., 2024), the tendency of the horizontal wind (TD) was decomposed into contributions from horizontal advection (HAD), vertical advection (VAD), pressure gradient force (PGF), Coriolis force (CF), and a friction/residual term (F_r), shown as Equation 4. To focus the diagnosis on the momentum balance along the primary jet axis, a coordinate rotation was applied to align the new coordinate axis with the main LLJ flow direction, shown as Equation 5 (Q. H. Zhang et al., 2003). The parameters of $\mathbf{V}$, p, Φ, and f are the horizontal winds, pressure, geopotential, and Coriolis coefficient, respectively. And where v' is the wind speed in the y' direction, φ represents the angle between y' and y axis. The detailed form of the momentum balance terms in this rotated coordinate system followed the methodology of Du et al. (2014).

All budget components in Equation 4 were computed based on hourly ERA5 reanalysis data. Site-specific rotation angles were assigned individually after combining the local wind field near the observation sites and the direction of the LLJ axis: 9π/25 for ES, π/4 for YC, and 3π/25 for WH. All differential operators required for momentum decomposition, including temporal differencing, horizontal advection (HAD), vertical advection (VAD), and pressure-gradient force (PGF) terms, were calculated using the central finite difference method. Following the calculation framework proposed in Zeng et al. (2019), the frictional term (Fr) was diagnosed residually by subtracting all other solved dynamic terms, which may be influenced by subgrid-scale processes. In addition, momentum budget components derived from ERA5 grid data were interpolated to the exact geographic coordinates of the three observational stations through bilinear spatial interpolation before subsequent composite and statistical analyses.

According to Blackadar (1957), the diurnal variation of LLJs can be explained by inertial oscillation mechanisms. Daytime vigorous vertical mixing within the boundary layer creates ageostrophic winds associated with their clockwise rotation. When inertial oscillation dominates such diurnal behavior, the summed contributions of PGF

21698996, 2026, 18, Downloaded from https://agupubs.onlinelibrary.wiley.com/doi/10.1029/2026JD047362, Wiley Online Library on [04/11/2026]. See the Terms and Conditions (https://onlinelibrary.wiley.com/terms-and-conditions) on Wiley Online Library for rules of use; OA articles are governed by the applicable Creative Commons License

and CF serve as the primary term in momentum balance, while the Fr frictional term acts to decelerate LLJs during daytime hours (Du et al., 2014).

$$\underset{\text{TD}}{\frac{\partial \boldsymbol{V}}{\partial t}} = \underset{\text{HAD}}{-\boldsymbol{V}_h \cdot \nabla_h \boldsymbol{V}} \underset{\text{VAD}}{-\omega \frac{\partial \boldsymbol{V}}{\partial p}} \underset{\text{PGF}}{-\nabla \varnothing} \underset{\text{CF}}{-f\boldsymbol{k} \times \boldsymbol{V}} \underset{\text{F}_\text{r}}{+\boldsymbol{F}_r} \tag{4}$$

$$v' = u \sin \varphi + v \cos \varphi \tag{5}$$

The apparent heat source Q_1 and the apparent moisture sink Q_2 were calculated following the method of Yanai et al. (1973) as shown in Equations 6 and 7, were used to reveal the diurnal variation mechanisms of the Western Pacific Subtropical High (WPSH). For the convenience of analysis, the deviation between Q_1 and Q_2 was defined as Q_3 in the present study.

$$Q_1 = c_p \left[\frac{\partial T}{\partial t} + V \cdot \nabla T + \left(\frac{p}{p_0} \right)^{\frac{R}{c_p}} \omega \frac{\partial \theta}{\partial p} \right] \tag{6}$$

$$Q_2 = -L \left(\frac{\partial q}{\partial t} + V \cdot \nabla q + \omega \frac{\partial q}{\partial p} \right) \tag{7}$$

where parameters of T, V, p, ω, θ, q are the temperature, horizontal winds, pressure, vertical velocity, potential temperature, and specific humidity. P_0, C_p, R and L are the reference pressure (1,000 hPa), specific heat of dry air at constant pressure, the gas constant for dry air and latent heat of condensation.

3. Results

3.1. Heterogeneity in LLJ Occurrence Heights Across Sub-Regions

The vertical distributions of LLJ occurrence frequency and mean wind speed exhibit pronounced topographic dependence across the MRYR transect, reflecting a clear topographic dependence (Figure 2). In the plain (WH), the occurrence frequency is characterized by a distinct double-peak pattern, with a primary peak occurring in the BLJ height range (~500–1,000 m AGL) and a secondary peak in the SLLJ layer (~2,000–2,500 m AGL). BLJs at WH are significantly more intense than SLLJs, a result consistently supported by mean wind speed statistics (median wind speeds, not shown, follow the same trend). This intensity relationship contrasts with that in the lower reaches of the Yangtze River, where SLLJs are stronger than BLJs (Du et al., 2012).

In the terrain-affected regions (ES and YC), the vertical distribution of LLJ is dominated by a single peak in the SLLJ layer (1.5–2.0 and 2.5–3.0 km AGL), showing a different pattern to that observed in the plain. These findings contrast with those of Zheng et al. (2026) and Shu et al. (2024), who reported that BLJs are active in mountainous regions. Moreover, the single-peak SLLJ morphology distinguishes the MRYR from other mountainous regions in China. For example, a double-peak distribution prevails in the North China mountain-plain transition zone (L. A. Zhou et al., 2024).

Wind speeds below 1,500 m AGL are markedly weaker than those aloft in the terrain-affected regions (Figure 2), a feature linked to the frictional drag induced by complex terrain. Meanwhile, the planetary boundary layer over mountainous terrain usually develops deeper, especially during daytime hours (Figure 7a), when significant contrasts are observed between the terrain-affected regions and the plain. A deep boundary layer is usually accompanied by intense vertical turbulent mixing, which homogenizes the vertical distribution of wind speed within the boundary layer (Bonner, 1968; Stull, 1988; W. Wei et al., 2013). Nevertheless, the formation of BLJs simultaneously requires two critical prerequisites: adequate wind speed magnitude and pronounced vertical wind shear. Therefore, these two physical processes (terrain drag and vertical turbulent mixing) drastically reduce BLJ occurrence frequency over the terrain-affected regions (ES and YC) relative to the plain.

To further validate the aforementioned daytime-enhanced turbulent mixing over mountainous terrain, we calculated the gradient Richardson number at 900 m AGL, a typical level of BLJ core height over the MRYR (Figure 7d), specifically during daytime hours when BLJs are still frequently observed over the plain but are

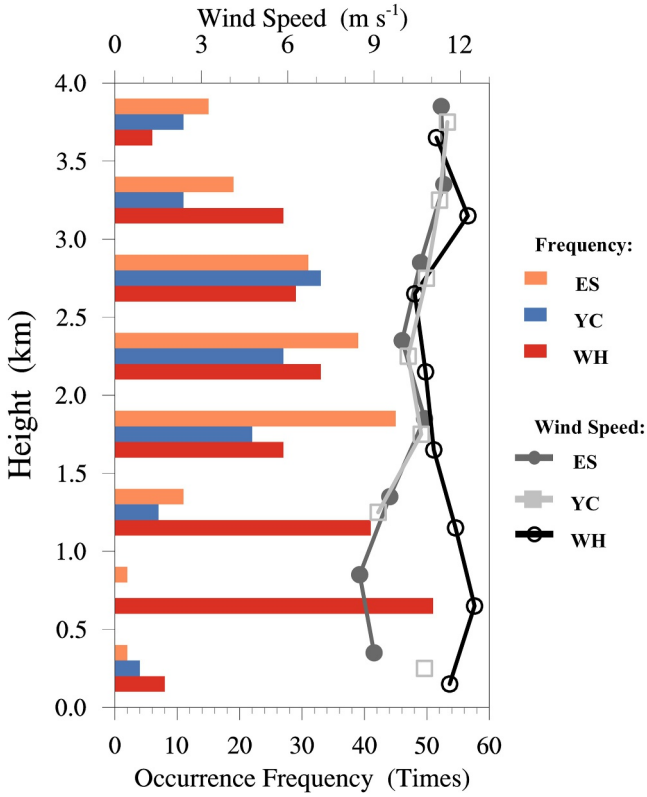


Figure 2. Vertical distributions of low-level jet occurrence frequency (bars, units: number of times) and the corresponding mean wind speeds (line with markers, units: m s^{-1}). Results are derived from intensive radiosonde observations at the three observational sites in this study.

nearly absent over the mountainous sites (Figure 3). The results show that the proportion of samples with a gradient Richardson number smaller than 0.25 at ES reaches 30.3%, higher than the 25.2% at WH, which further confirms that the turbulence is more easily generated and sustained in terrain-affected regions (Wang et al., 2020), indirectly suggesting the more vigorous turbulent mixing within the mountain boundary layer.

In summary, LLJs over the MRYR exhibit strong regional features in both vertical structure and intensity. The contrasting single- versus double-peak vertical distributions form a distinctive regime, driven by the unique topographic and synoptic setting of the MRYR (W. Wei et al., 2014).

3.2. Sub-Regional Differences in Diurnal Cycles of LLJ Frequency

Among the three sites, LLJs occur most frequently in the plain region (WH), followed by the mountainous region (ES), though the underlying reasons for their high frequencies differ. At WH, the high frequency arises from both BLJs and SLLJs (Figure 3c). At ES, by contrast, frequent SLLJs are the dominant contributor (Figure 3a). In comparison, DLLJs are active at WH (Figure 3c), they rarely occur over terrain-affected regions (ES and YC), where BLJs show much lower occurrence rates (Figures 3a and 3b).

Figure 3d compares the frequent LLJ subtypes across the three sites. Unlike the weak diurnal cycles of SLLJs reported in other regions of China (Du et al., 2012), SLLJs over the MRYR exhibit pronounced diurnal variations. Quantitatively, the diurnal cycle of SLLJs is strongest in the mountain-plain transition region (YC), with a Pearson correlation coefficient of 0.803 (significant at the 90% confidence level). Moreover, the diurnal pattern of SLLJs varies by sites. The frequency peaks at 08:00 LST in the plain, but during nighttime hours (02:00–05:00 LST) in the terrain-affected regions.

A clear double-peak diurnal pattern of BLJs appears at WH, with the primary at 23:00 LST and a secondary peak at 08:00 LST. This contrasts with the predominantly single-peak pattern reported for BLJs in other regions of China (Du & Chen, 2019; Du et al., 2014, 2022; Shu et al., 2024). At WH, because both BLJs and SLLJs peak at 08:00 LST at WH, the total LLJ occurrence rate reaches its daily maximum at this hour (Figure 3c).

3.3. Contrasting Diurnal Variations of the Fine-Scale Vertical Structure of LLJs

Previous investigations into the vertical structure of LLJs have largely relied on composite analyses of LLJ events (Du & Chen, 2019; Du et al., 2022), due to the scarcity of high-resolution vertical observations. Even when observational profiles are available, most studies have focused on the diurnal variations in LLJ intensity at a single site (C. Cui et al., 2023; X. Zhang et al., 2024), with less attention given to the diurnal evolution of LLJ core height. This study takes advantage of high-temporal-resolution multi-site vertical observations along the MRYR transect to examine the diurnal characteristics of LLJ vertical structure, with a particular emphasis on LLJ core height variations.

Among the three sites, the diurnal patterns of SLLJ and BLJ intensity are most pronounced at WH, where SLLJs reach their maximum intensity during the day and BLJs at night (Figures 4c and 4d), consistent with the daytime frequency peak of SLLJs and nighttime frequency peak of BLJs at this site (Figure 3d). Notably, the diurnal cycles of SLLJ height are evident at all three sites but exhibit systematic differences between the plain and the terrain-affected regions (Figures 4a, 4b, and 4d).

Specifically, at ES and YC, the SLLJ core height descends from 20:00 to 02:00 LST (accompanied by jet intensification) and then ascends from 02:00 to 17:00 LST (Figures 4a and 4b), resulting in a higher daytime SLLJ core height in the terrain-affected regions (Figure 4e). In stark contrast, the descending periods of SLLJs at WH lasts longer (from 20:00 to 08:00 LST) alongside significant SLLJ intensification (Figure 4d), leading to a lower daytime SLLJ core height at this site (Figure 4e). Notably, the diurnal pattern of SLLJ height at the terrain-

21698996, 2026, 18, Downloaded from https://agupubs.onlinelibrary.wiley.com/doi/10.1029/2026JD047362, Wiley Online Library on [04/11/2026]. See the Terms and Conditions (https://onlinelibrary.wiley.com/terms-and-conditions) on Wiley Online Library for rules of use; OA articles are governed by the applicable Creative Commons License

21698996, 2026, 18, Downloaded from https://agupubs.onlinelibrary.wiley.com/doi/10.1029/2026JD047362, Wiley Online Library on [04/11/2026]. See the Terms and Conditions (https://onlinelibrary.wiley.com/terms-and-conditions) on Wiley Online Library for rules of use; OA articles are governed by the applicable Creative Commons License

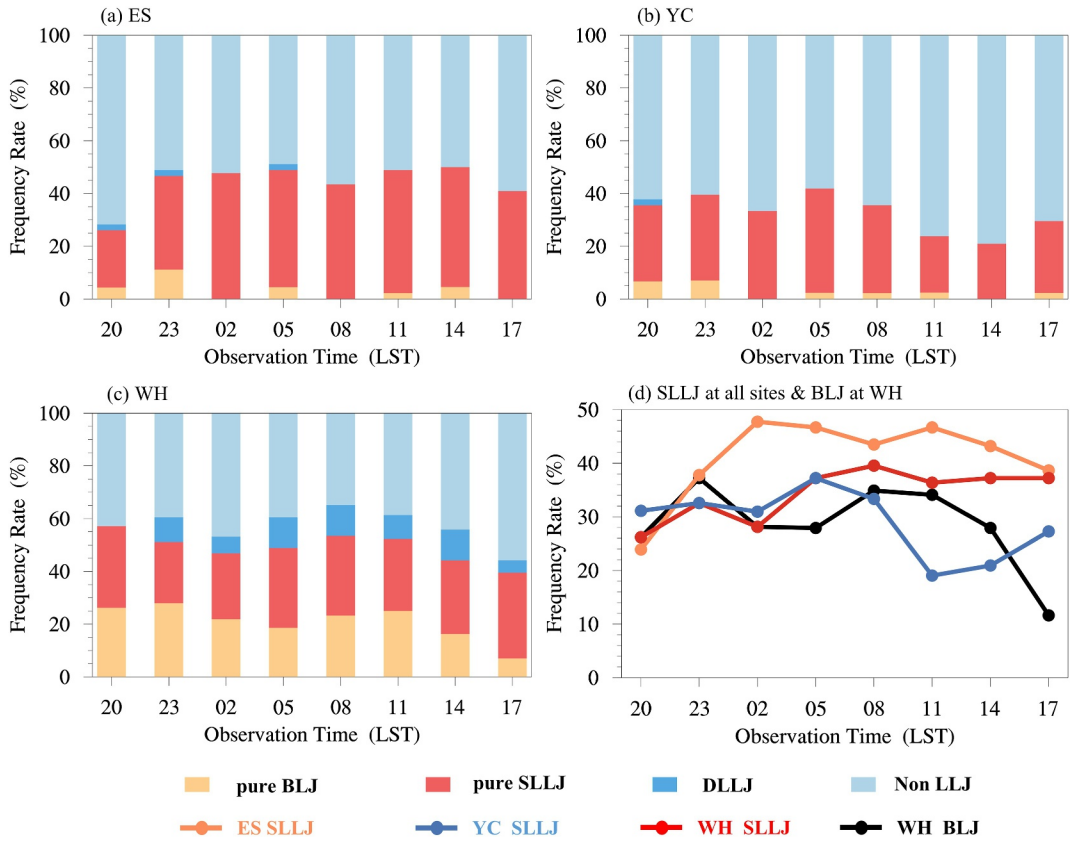


Figure 3. (a–c) Diurnal variations of occurrence rates (bars, units: %) for pure boundary-layer jet (BLJ) (orange), pure SLLJ (red), DLLJ (blue), and non-LLJ (light blue) observations at three sites. (d) Diurnal cycle of total SLLJ and BLJ occurrences (line with markers, units: %).

affected sites resembles that of LLJ height at the plain region (Figure 4c), suggesting that the SLLJ identification in terrain-affected regions may include some BLJ samples, a point that will be further supported in Section 3.5.

3.4. Validation of ERA5 for Capturing Sub-Regional LLJ Diurnal Behaviors

To diagnose the mechanisms governing the diurnal variations of SLLJs under different terrain conditions across the MRYR region, we conducted a momentum budget analysis using the ERA5 reanalysis data set. Before this analysis, we first evaluated ERA5's capability to capture the key diurnal characteristics of SLLJs across this region.

The low-level winds from ERA5 were compared with radiosonde observations (Figures 5–7). The root-mean-square error (RMSE) values of low-level wind speeds range from 1.779 to 2.136 m s^{-1} (Figure 5), indicating that ERA5 generally reproduces the regional wind field with reasonable accuracy. More critically, ERA5 robustly reproduces the composite "nose-shaped" vertical profile of observed pure SLLJs and BLJs (Figure 6). The ability of ERA5 to represent LLJ wind speed has also been confirmed by Lima et al. (2022).

The composite SLLJ and BLJ profiles in Figure 4 are constructed from non-consecutive observation times and are therefore unsuitable for momentum budget analysis, which requires temporally continuous data. To overcome this limitation, we adopted the concept of an "SLLJ day" and "BLJ day" from Du et al. (2014). Here, an SLLJ or BLJ day is identified as a day on which the corresponding criteria are met during at least one-quarter of the daily observation times (e.g., ≥2 out of 8 daily intensive radiosonde observations in this study). We further assessed whether the continuous wind field from such days retains the key diurnal signals of the intermittent pure SLLJ and BLJ composites derived from observational profiles. A comparison between the diurnal composites based on this definition (Figures 7a–7d) and the pure SLLJ and BLJ composites (Figures 4a, 4b, 4d, and 4e) shows consistent representation of key features, including the evolution of jet core height, confirming the validity of this approach.

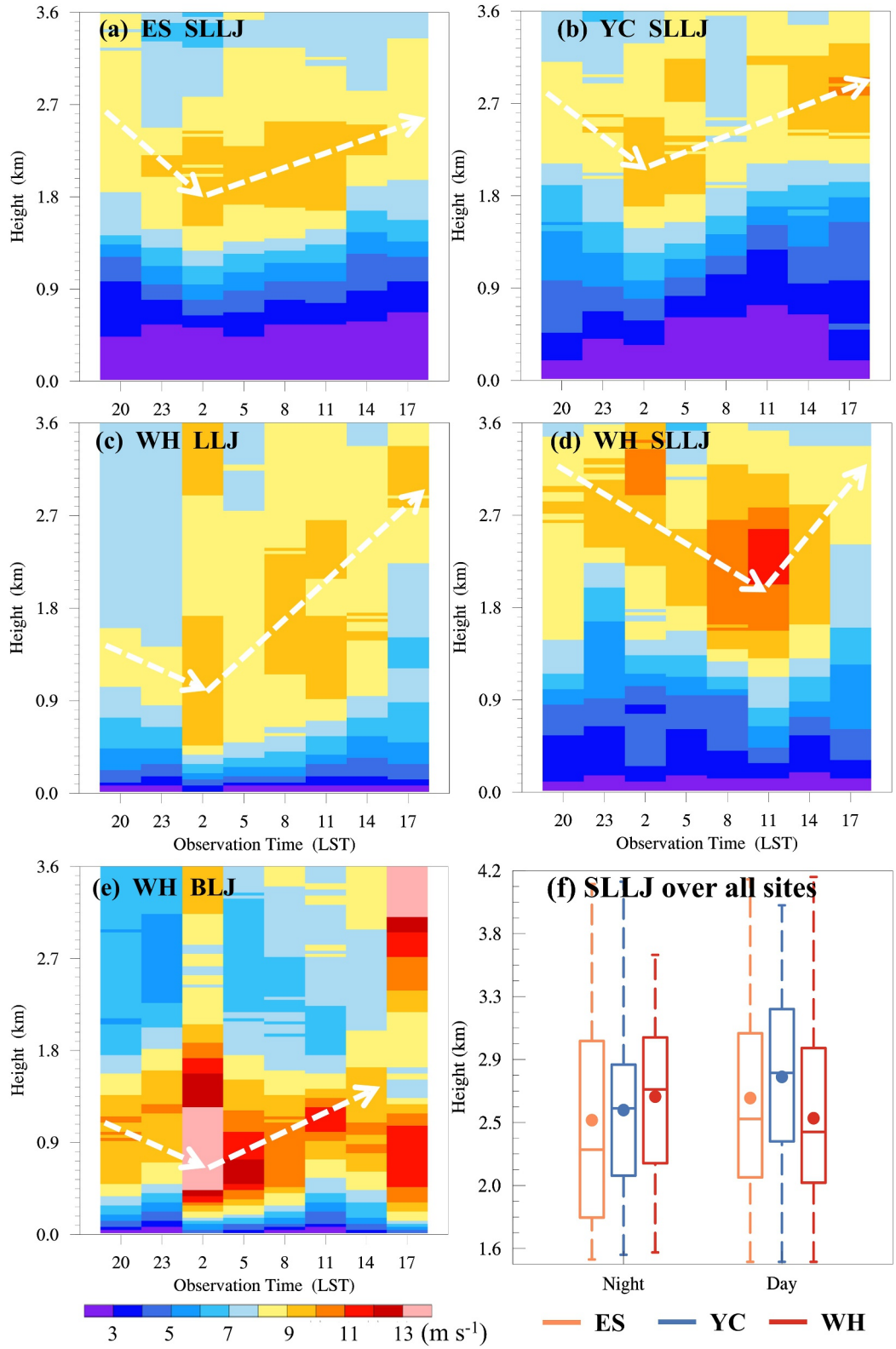


Figure 4. (a and b) Diurnal variations of the fine-scale wind speed (shading, units: m s^{-1}) vertical structures during pure SLLJ observations at ES and YC. Panels (c–e) are the same as panels (a and b), except for low-level jet, pure SLLJ, and pure boundary-layer jet observations at WH. The white dashed lines illustrate the variation trend of jet core height. Panel (f) provides the box-and-whisker plot of SLLJ core height during nighttime and daytime periods.

21698996, 2026, 18, Downloaded from https://agupubs.onlinelibrary.wiley.com/doi/10.1029/2026JD047362, Wiley Online Library on [04/11/2026]. See the Terms and Conditions (https://onlinelibrary.wiley.com/terms-and-conditions) on Wiley Online Library for rules of use; OA articles are governed by the applicable Creative Commons License

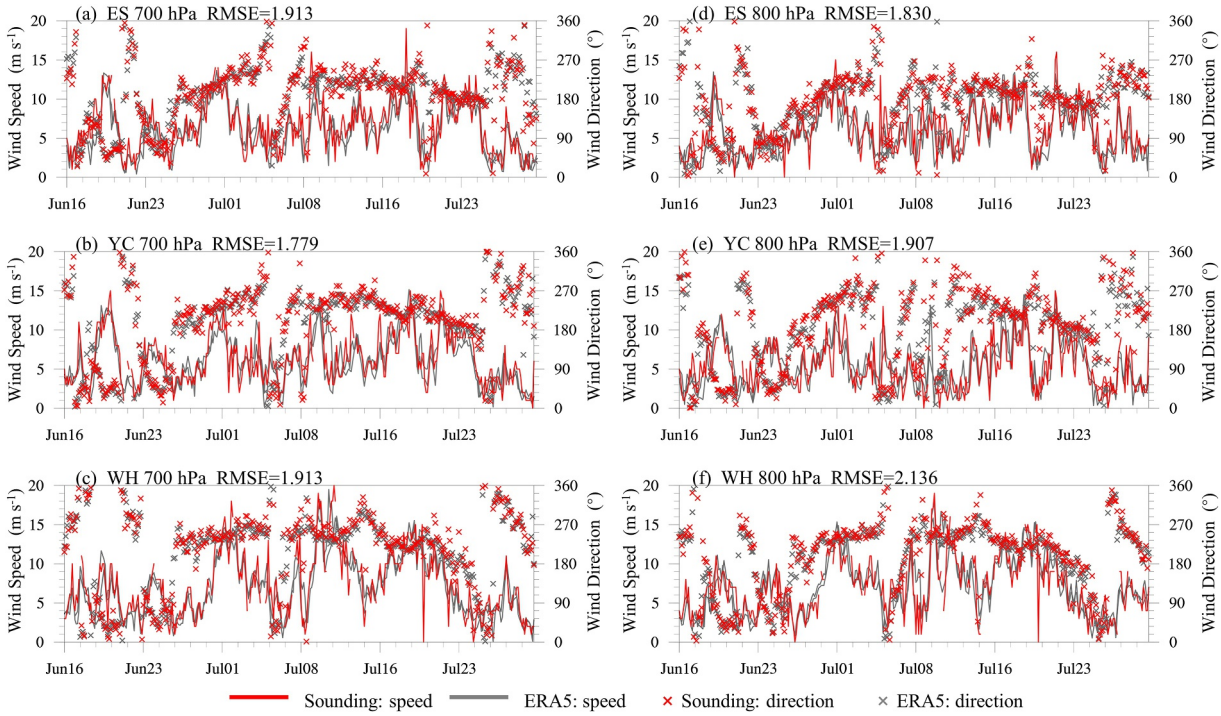


Figure 5. Time series of wind speeds (lines, units: m s^{-1}) and wind directions (crosses, units: °) at (a–c) 700 hPa and (d–f) 800 hPa from radiosonde observations (red) and ERA5 reanalysis (gray).

This consistency holds even under a stricter criterion (e.g., ≥4 out of 8 observations; relevant figures can be found in Supporting Information S1). Therefore, data from such days provide a suitable and temporally continuous basis for the subsequent mechanism diagnosis.

We then evaluated ERA5's performance on the same SLLJ days and BLJ days (Figures 7e–7g) by comparing them with observations (Figures 7a–7d). Results indicate that ERA5 generally captures the diurnal evolution of the SLLJ and BLJ vertical structure. For instance, ERA5 reproduces the upward trend of SLLJ core height starting around 02:00 LST, as well as the nighttime (02:00–05:00 LST) and daytime (11:00–14:00 LST) wind speed maxima, albeit with a slight underestimation of wind speed. In the plain region, ERA5 performs well in depicting the longer descent period of SLLJ core height, which continues until approximately 08:00 LST. ERA5 data also captures the stronger daytime (nocturnal) SLLJ (BLJ) intensity (Figure 7g) at WH (Figure 7h).

In summary, despite minor intensity discrepancies, ERA5 reanalysis data demonstrate sufficient reliability in capturing the key diurnal variation characteristics of LLJs over the MRYR region. These validations support the applicability of the ERA5 data set for the subsequent quantitative momentum budget analysis.

3.5. Mechanisms Governing Sub-Regional Differences in LLJ Diurnal Behaviors

To understand the physical mechanisms governing sub-regional differences in LLJ diurnal behaviors, we examined three complementary aspects: (a) the role of boundary layer thermal structure in modulating LLJ core height, (b) the influence of synoptic-scale weather systems on LLJ intensity, and (c) the momentum budget terms that quantify the dominant physical processes.

3.5.1. Mechanisms for Diurnal Variations of LLJ Core Height

As shown in Figures 7a–7d, SLLJ core heights are consistently higher than the PBLH, whereas BLJ core heights lie below the PBLH, confirming that the LLJ identification over the MRYR is generally robust. The diurnal variations of SLLJ core height in the terrain-affected regions (ES and YC) and BLJ core height in the plain region (WH) exhibit consistent trends with the PBLH, suggesting a pronounced influence of boundary layer processes on

21698996, 2026, 18, Downloaded from https://agupubs.onlinelibrary.wiley.com/doi/10.1029/2026JD047362, Wiley Online Library on [04/11/2026]. See the Terms and Conditions (https://onlinelibrary.wiley.com/terms-and-conditions) on Wiley Online Library for rules of use; OA articles are governed by the applicable Creative Commons License

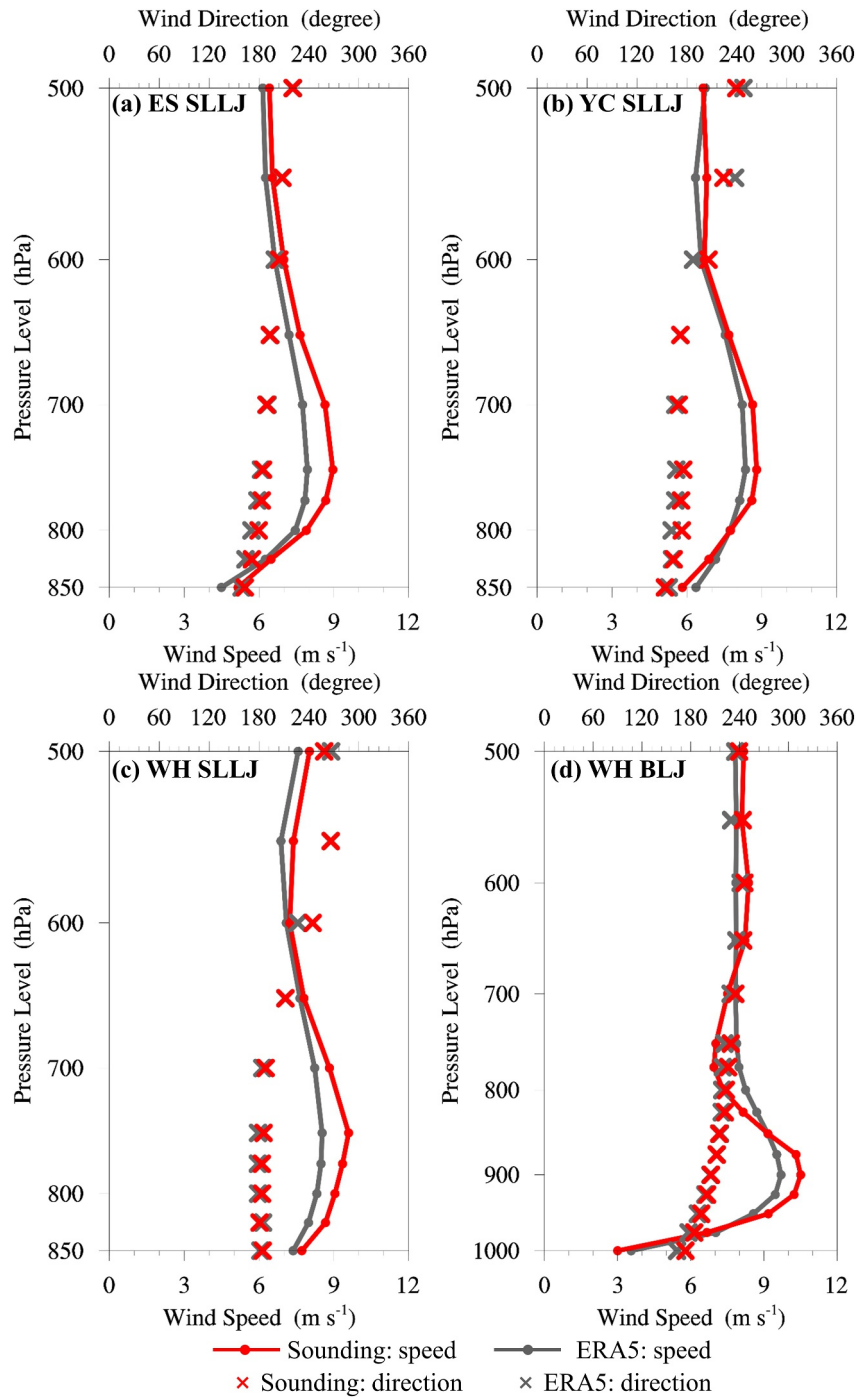


Figure 6. Composite profiles of wind speed (line with markers, units: m s^{-1}) and wind direction (crosses, units: °) for pure (a–c) SLLJ and (d) boundary-layer jet (BLJ) observations. Profiles are composited over all valid vertical profiles identified as pure SLLJ or BLJ observations during the 2010 Mei-yu field campaign, based on radiosonde observations. Red and dark gray represent data collected from intensive radiosonde observations and ERA5 reanalysis, respectively.

jet core height (Rotach & Zardi, 2007). In contrast, the relationship between SLLJ core height and PBLH at WH is relatively weaker.

It can be observed that the PBLH develops higher in the terrain-affected regions than that in the plain region (black lines in Figures 7a–7c), owing to the topographic thermal forcing over complex terrain (Figure 8a).

21698996, 2026, 18, Downloaded from https://agupubs.onlinelibrary.wiley.com/doi/10.1029/2026JD047362, Wiley Online Library on [04/11/2026]. See the Terms and Conditions (https://onlinelibrary.wiley.com/terms-and-conditions) on Wiley Online Library for rules of use; OA articles are governed by the applicable Creative Commons License

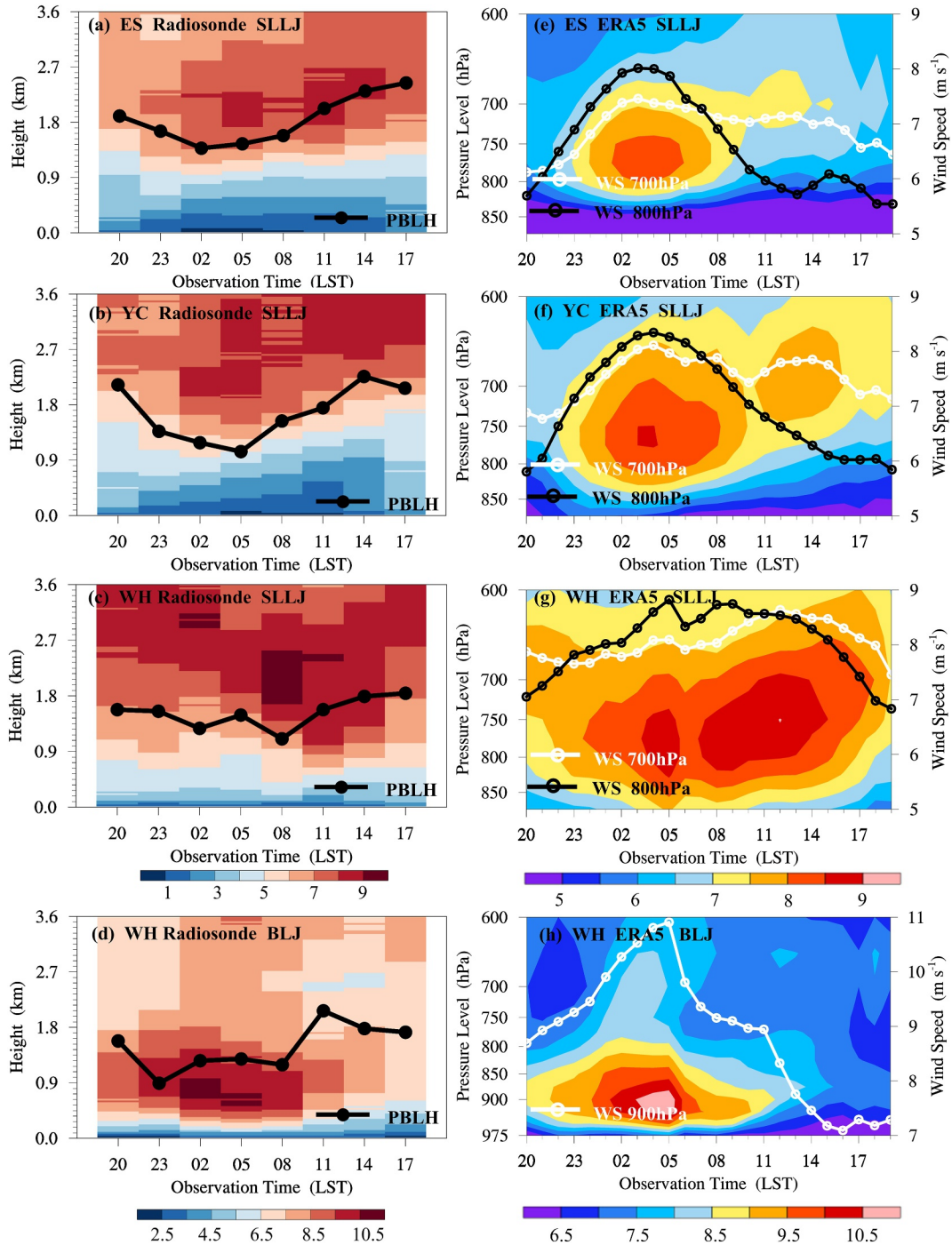


Figure 7. Diurnal variations of PBLH (line with markers, units: km) and vertical structures of horizontal wind speeds (shading, units: m s^{-1}) based on intensive radiosonde data during (a–c) SLLJ and (d) boundary-layer jet (BLJ) days. Black lines with markers indicate PBLH (units: km). (e–h) Diurnal variations of vertical structures of horizontal wind speeds from ERA5 data for the same SLLJ and BLJ days. White and black lines with markers in panels (e–g) indicate wind speeds (units: m s^{-1}) at 700 hPa and at 800 hPa, respectively. White lines with markers in panels (h) indicate wind speeds (units: m s^{-1}) at 900 hPa.

Consequently, BLJs may develop at higher altitudes in these regions. Furthermore, the secondary-step terrain of the MRYR is frequently influenced by the Southwest Vortex (Figure S1 in Supporting Information S1), whose typical activity levels lie between 750 and 800 hPa (Fu et al., 2022; Y. C. Zhang et al., 2019), leading to frequent

21698996, 2026, 18, Downloaded from https://agupubs.onlinelibrary.wiley.com/doi/10.1029/2026JD047362, Wiley Online Library on [04/11/2026]. See the Terms and Conditions (https://onlinelibrary.wiley.com/terms-and-conditions) on Wiley Online Library for rules of use; OA articles are governed by the applicable Creative Commons License

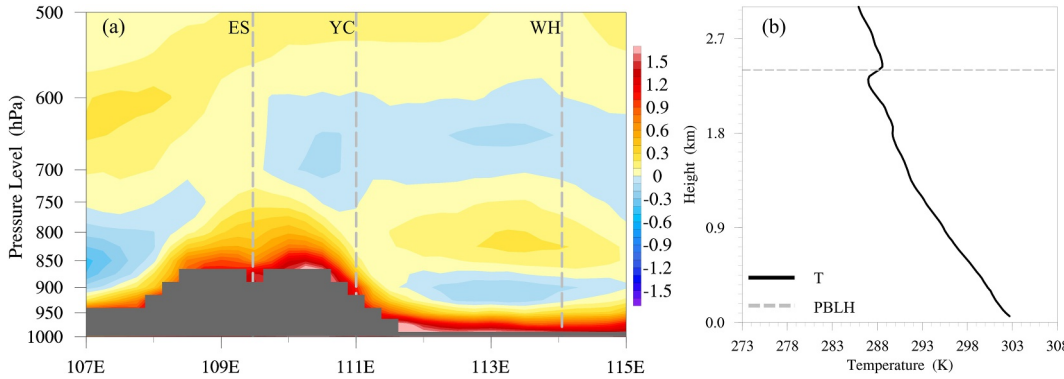


Figure 8. (a) Vertical cross sections of the deviations between daytime and nighttime zonal-mean potential temperature (color shading, units: K) averaged over 30°–31°N. Dark gray shading denotes topography. Dashed lines from west to east indicate the locations of ES, YC, and WH, respectively. (b)The temperature profile (black lines, units: K) and corresponding boundary layer height at 11:00 LST 1 July 2010, derived from the radiosonde observations in ES. Note that smoothing is applied to the temperature profile. This operation primarily removes random local noise originating from instrument measurement errors and numerical differentiation, which could produce spurious sharp gradient peaks and induce erroneous PBLH estimation.

SLLJ activity at these levels. This poses challenges in distinguishing true SLLJs from BLJs over these regions. In other words, SLLJs at ES and YC may include some higher-altitude BLJ samples, resulting in a closer relationship between SLLJ core height and PBLH.

Mechanistically, the boundary layer top is characterized by a capping inversion (Figure 8b), a stable layer that inhibits the downward transfer of momentum from the free atmosphere to the boundary layer. As a result, a zone of stronger momentum is maintained immediately above the boundary layer top (Stull, 1988). The diurnal growth and collapse of the PBLH, which can be significantly modified by terrain-driven thermal heterogeneities and mechanical mixing, effectively lifts or depresses this overlying strong momentum zone. This process thereby dictates the SLLJ core height.

Conversely, in the plain site (WH), the local coupling between SLLJ and PBLH is not as strong as that in the terrain-affected sites. The PBLH exhibits a relatively weaker diurnal variation, whereas the SLLJ core height changes markedly (Figure 7c), which indicates that the evolution of SLLJs in the plain is governed less by local boundary-layer forcing and more by large-scale synoptic forcing (C. Cui et al., 2023; Du et al., 2014; Shu et al., 2024). An analysis of the Mei-yu front reveals that the descent and ascent of the SLLJ core height at WH are associated with the intensification of the Mei-yu front at 800 hPa and 700 hPa, respectively (Figure 9). Specifically, frontal condensation initiates in the early morning, intensifying the Mei-yu front and the southerly winds at low levels near 800 hPa (W. Cui et al., 2020; Hu et al., 2021, 2022). As convective condensation gradually

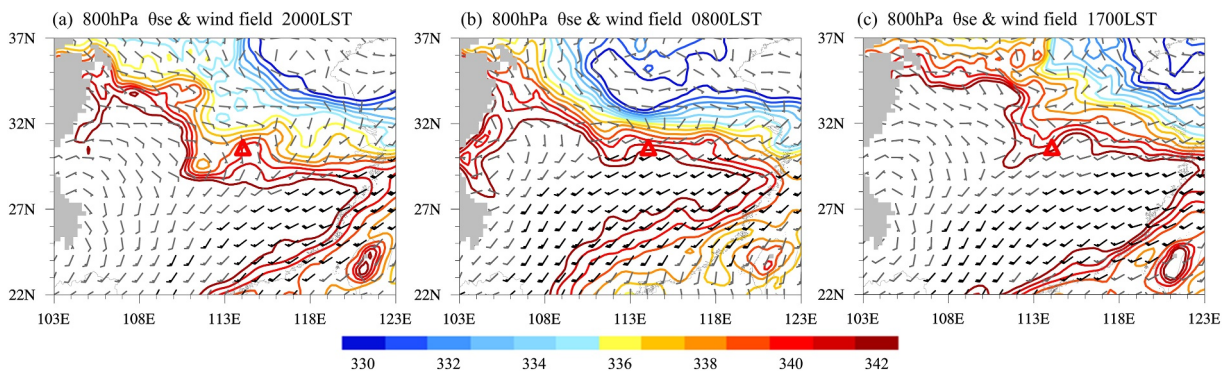


Figure 9. Composite-average spatial distributions of 800-hPa pseudo-equivalent potential temperature (contours, units: K) and wind field (wind barbs, units: m s^{-1}, black wind barbs represent wind speeds larger than 6 m s^{-1}) at (a) 20:00 LST, (b) 08:00 LST, (c) and 17:00 LST during SLLJ observations at WH. Gray shading represents topography, and the red triangle represents the location of WH.

21698996, 2026, 18, Downloaded from https://agupubs.onlinelibrary.wiley.com/doi/10.1029/2026JD047362, Wiley Online Library on [04/11/2026]. See the Terms and Conditions (https://onlinelibrary.wiley.com/terms-and-conditions) on Wiley Online Library for rules of use; OA articles are governed by the applicable Creative Commons License

21698996, 2026, 18, Downloaded from https://agupubs.onlinelibrary.wiley.com/doi/10.1029/2026JD047362, Wiley Online Library on [04/11/2026]. See the Terms and Conditions (https://onlinelibrary.wiley.com/terms-and-conditions) on Wiley Online Library for rules of use; OA articles are governed by the applicable Creative Commons License

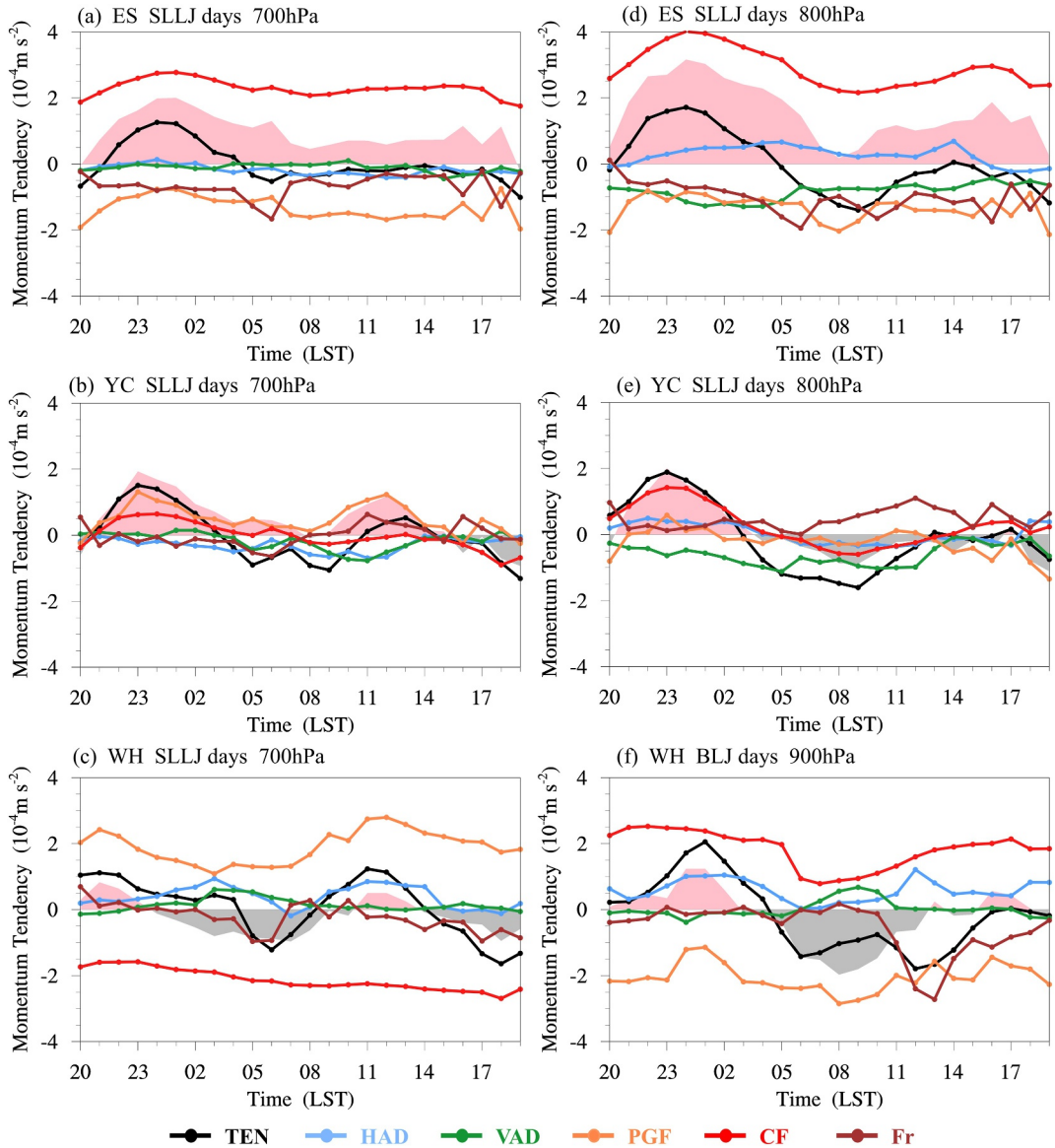


Figure 10. Diurnal variations of momentum budget terms (lines with markers, in 10^{-4} m s^{-2}) at different observation sites: (a–c) 700 hPa at ES, YC and WH during SLLJ days. Panels (d and e) are the same as panels (a and b), except for analysis at 800 hPa. Panel (d) indicates diurnal variations of momentum budget (lines with markers, in 10^{-4} m s^{-2}) at 900 hPa at WH during boundary-layer jet days. Shading indicates the sum of the pressure gradient force and Coriolis force, with pink and gray representing positive and negative values, respectively.

becomes dominant in the afternoon, the levels of maximum frontal and southerly wind responses shift upward accordingly.

3.5.2. Mechanisms for Diurnal Variations of LLJ Frequency and Intensity

Figure 10 shows that the wind speeds in the terrain-affected regions undergo significant nocturnal acceleration (black lines), with the acceleration rate reaching a peak around 23:00–02:00 LST, approximately 3 hr ahead of the wind speed peak (Figures 7e and 7f). The budget terms at YC are similar to the results at ES but with smaller magnitudes. Therefore, the following analysis about the terrain-affected regions mainly focuses on the results at ES.

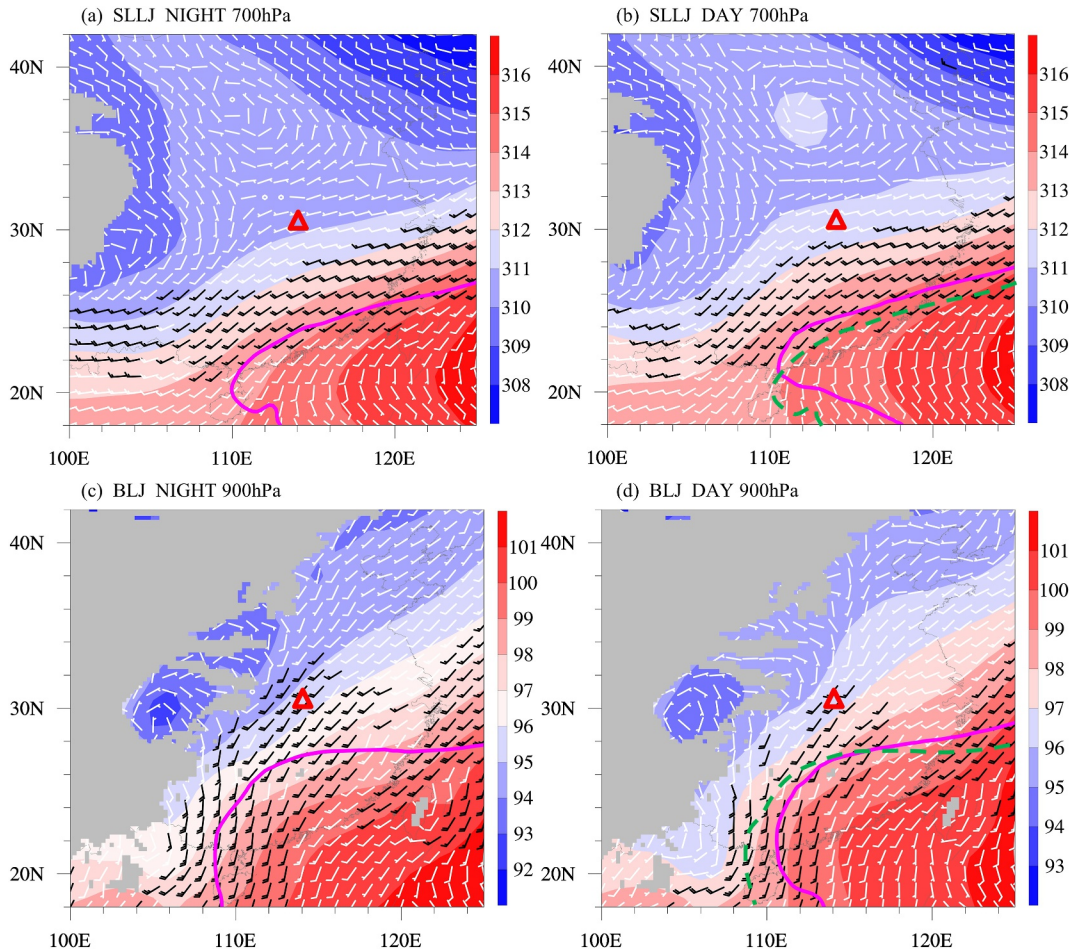


Figure 11. (a) Nighttime and (b) daytime composite-average spatial distributions of 700-hPa geopotential height (shadings, units: dagpm), horizontal wind field (wind barbs, units: m s^{-1}, black wind barbs represent wind speeds larger than 6 m s^{-1}), and the 588-dagpm contour (magenta contours, units: dagpm) at 500 hPa during SLLJ observations at WH. Panels (c and d) are the same as panels (a and b), except at 900 hPa during the boundary-layer jet observations. To show the variations of the WPSH, the nighttime 588-dagpm contours in panels (a and c) have also been plotted as green dashed contours in panels (b and d).

At 700 hPa (Figure 10a), the HAD and VAD terms are relatively small. The wind acceleration rate closely follows the CF term, whereas the PGF term varies little. The imbalance between the CF and PGF terms peaks precisely at the same time as the wind acceleration rate, indicating that the inertial oscillation is the primary driver of nocturnal SLLJ intensification in the terrain-affected regions (Blackadar, 1957; Du & Rotunno, 2014; Shapiro et al., 2016). This contrasts with SLLJs over other regions of China, which are mainly modulated by synoptic weather systems (Du & Chen, 2019; Du et al., 2014; W. Wei et al., 2014). Notably, at 800 hPa the inertial oscillation is even more pronounced (Figure 10d), because this level is closer to the boundary layer and thus more strongly affected by boundary layer processes. The distinct inertial oscillation signatures at both 700 hPa and 800 hPa further confirm that boundary layer processes play a key role in modulating SLLJ core height in the terrain-affected regions. Moreover, the VAD and HAD terms are considerably larger at 800 hPa than at 700 hPa, indicating more vigorous vertical and horizontal momentum transport at this level. The 800-hPa Fr term holds greater absolute values during daytime hours than at night (Figure 10d). This dominant daytime frictional effect decelerates wind speeds, which may be attributed to vigorous vertical momentum mixing within the boundary layer (Du et al., 2014).

For SLLJs in the plain region (WH), the daytime wind acceleration is closely tied to a pronounced daytime strengthening of the PGF term, which overwhelms the variation in the CF term (Figure 10c). This daytime PGF enhancement is dynamically linked to the northward advance of the Western Pacific Subtropical High (WPSH; Figures 11a and 11b), which in turn is closely associated with the daytime land heating (Figure 12), particularly

21698996, 2026, 18, Downloaded from https://agupubs.onlinelibrary.wiley.com/doi/10.1029/2026JD047362, Wiley Online Library on [04/11/2026]. See the Terms and Conditions (https://onlinelibrary.wiley.com/terms-and-conditions) on Wiley Online Library for rules of use; OA articles are governed by the applicable Creative Commons License

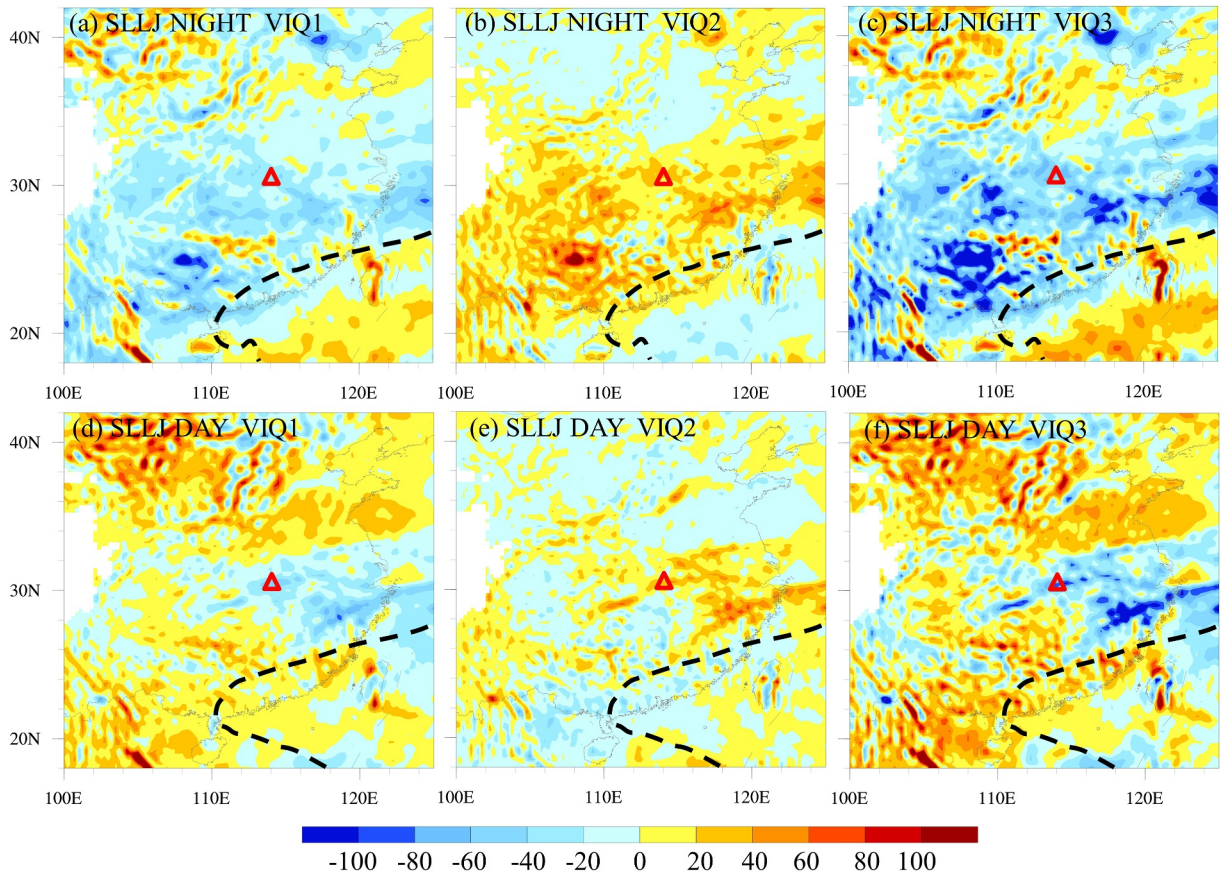


Figure 12. (a) Nighttime and (d) daytime composite-average spatial distributions of vertically integrated apparent heat source Q_1 (shading, units: W m^{-2}) from the surface to 500 hPa during SLLJ observations. Middle and right panels are the same as left panels (a, d), but show the apparent moisture sink Q_2 in panels (b, e) and Q_3 in panels (c, f). Black dashed contours indicate the 588-dagpm contours.

sensible and radiative heating (Figure 12f). Together, these results highlight the direct role of synoptic-system forcing in modulating SLLJ intensities in the plain region.

As for the nocturnal BLJ intensity and occurrence peak at WH, it is mainly governed by the inertial oscillation (Figure 10f). Unlike SLLJs, BLJs are also influenced by the WPSH, but through its westward extension (Figures 11c and 11d). Furthermore, coupled with the nocturnal development of southwest vortices (Figures 11a and 11c), the pressure gradient exhibits a larger magnitude at night. Superimposed on the pronounced inertial oscillation, this leads to a greater BLJ intensity than that of SLLJs in the plain region.

4. Conclusions and Discussions

The evolution of LLJs exerts a significant influence on the development and spatial distribution of heavy rainfall. Consequently, considerable efforts have been devoted to understanding LLJ characteristics and their underlying mechanisms. However, most previous studies have focused on single sites or on comparisons across regions with large-scale climatic contrasts, leaving sub-regional differences in the diurnal characteristics of LLJs and their governing mechanisms largely unexplored.

The MRYR is a high-frequency LLJ region characterized by a heterogeneous mosaic of plains, hills, and mountains. This complex terrain, coupled with the presence of active weather systems, produces substantial variability in the low-level wind field. Utilizing a unique data set of synchronous intensive radiosonde observations from three representative sites across the MRYR during the 2010 Mei-yu period, combined with ERA5 reanalysis data and momentum budget diagnostics, this study systematically investigates sub-regional differences in LLJ vertical structure, diurnal variations, and underlying mechanisms. The principal findings are summarized as follows.

21698996, 2026, 18, Downloaded from https://agupubs.onlinelibrary.wiley.com/doi/10.1029/2026JD047362, Wiley Online Library on [04/11/2026]. See the Terms and Conditions (https://onlinelibrary.wiley.com/terms-and-conditions) on Wiley Online Library for rules of use; OA articles are governed by the applicable Creative Commons License

21698996, 2026, 18, Downloaded from https://agupubs.onlinelibrary.wiley.com/doi/10.1029/2026JD047362, Wiley Online Library on [04/11/2026]. See the Terms and Conditions (https://onlinelibrary.wiley.com/terms-and-conditions) on Wiley Online Library for rules of use; OA articles are governed by the applicable Creative Commons License

In terrain-affected regions (ES and YC), LLJ occurrence heights exhibit a single-peak vertical distribution, predominantly between 1.5 and 2.5 km AGL, indicating the dominance of SLLJs. In contrast, the plain region (WH) displays an evident double-peak structure, with the primary and secondary peaks occurring near 0.5–1.0 km AGL and 2.0–2.5 km AGL, respectively, reflecting a higher frequency of BLJs. In this plain, BLJs are stronger than SLLJs, differing from both terrain-affected regions and other plain regions of China.

The diurnal cycle of LLJs is strongly topography-dependent. In terrain-affected regions (ES and YC), SLLJ frequency and intensity peak at night (02:00–05:00 LST), primarily governed by nocturnal inertial oscillation under relatively higher planetary boundary layer height (PBLH). This behavior differs significantly from SLLJs in other regions of China. Conversely, over the plain, SLLJs occur more frequently during the daytime, peaking around 08:00 LST, and are mainly influenced by the northward advance of the WPSH, which intensifies the pressure gradient in the daytime. BLJs over the plain peak at night under the influence of inertial oscillation, consistent with typical BLJ behavior in China, and their intensification is additionally associated with the nocturnal westward extension of the WPSH.

The diurnal variations of SLLJ core height also differ among regions. In terrain-affected regions, the SLLJ core descends from 20:00 to 02:00 LST and then ascends from 02:00 to 17:00 LST, closely linked to diurnal PBLH variations. A capping inversion near the PBL top inhibits momentum transfer from the free atmosphere to the boundary layer, thereby maintaining a strong momentum layer aloft that shifts vertically with the evolution of PBLH. Over the plain, the nocturnal descent phase of SLLJ heights lasts longer (from 20:00 to 08:00 LST), associated with the strengthening of the Mei-yu front at 800 hPa during this period.

This study provides a comprehensive analysis of sub-regional differences in LLJ characteristics and their driving mechanisms across the MRYR. It advances existing LLJ research over the Yangtze River basin in three major respects relative to previous studies. First, we deployed synchronous radiosonde observations spanning mountains, transition zone, and plains to construct a complete terrain transect, which enables the separation of terrain signals unavailable from the single-site measurements or large-scale climatic contrasts adopted in prior studies (C. Cui et al., 2023; Du & Chen, 2019; Du et al., 2014; W. Wei et al., 2014; C. Zhou et al., 2026). Second, we identify distinct diurnal shifting patterns of jet core height under different terrain conditions. Such fine-scale vertical diurnal differences have not been systematically explored in earlier work, which mainly focused on LLJ frequency and synoptic variations (Miao et al., 2018; Yan et al., 2021; C. Zhou et al., 2026). Third, quantitative momentum budget diagnoses and composite analyses reveal terrain-dependent dominant dynamical pathways, including the boundary-layer processes on the evolution of SLLJs over the terrain-affected regions and the different modulation pathways of WPSH on the development of SLLJs and BLJs over the plain. This terrain-dependent divergence in dominant LLJ mechanisms has not been clearly distinguished in prior work (C. Cui et al., 2023; Du et al., 2012, 2014; Xue et al., 2018; Zeng et al., 2019; L. A. Zhou et al., 2024).

Nevertheless, our observational data set is limited to the 2010 Mei-yu season alone. Given that LLJ behaviors can be modulated by interannual circulation variability, multi-year observations and numerical simulations would therefore be valuable for extending LLJ understanding. In addition, constrained by the 3-hourly temporal resolution of the radiosonde data, we are unable to directly quantify turbulent mixing intensity in the present analysis. In future work, numerical sensitivity experiments targeting key parameters such as the turbulent diffusion coefficient may help better constrain the suppressive effect of turbulent mixing over mountainous regions on BLJs and unpack its underlying physical mechanisms. Furthermore, semi-idealized numerical simulations offer an opportunity to isolate topographic forcing from synoptic-scale background forcing, which would allow us to further disentangle their respective roles in shaping the diurnal-cycle variations of LLJs.

Conflict of Interest

The authors declare no conflicts of interest relevant to this study.

Availability Statement

The global topography data set is obtained from NOAA National Centers for Environmental Information (2022; https://www.ngdc.noaa.gov/mgg/global/global.html). The ERA5 reanalysis data are available at Hersbach et al. (2020; https://cds.climate.copernicus.eu/cdsapp#!/dataset/). The intensive radiosonde observation data are

obtained from China's National Meteorological Data Center (CMA, 2023; http://data.cma.cn/en/?r=data/detail&dataCode=B.0011.0001C) and also archived in Zenodo (https://doi.org/10.5281/zenodo.21636382).

Acknowledgments
This work is supported by the National Natural Science Foundation of China (Grants 42475018, 42625501, 42230612, 42475002), the Natural Science Foundation of Hubei Province (2025AFD422, 2024AFD209, 2024AFD217), the Open Fund Project for Heavy Rain (BYKJ2025Q33, BYKJ2025M26, BYKJ2024Z01), Open Research Fund of Heavy Rain and Drought-Flood Disasters in Plateau and Basin Key Laboratory of Sichuan Province (SZKT202509).

References

Bell, T. L., & Reid, N. (1993). Detecting the diurnal cycle of rainfall using satellite observations. *Journal of Applied Meteorology and Climatology*, *32*(2), 311–322. https://doi.org/10.1175/1520-0450(1993)032<0311:DTDCOR>2.0.CO;2

Blackadar, A. K. (1957). Boundary layer wind maxima and their significance for the growth of nocturnal inversions. *Bulletin of the American Meteorological Society*, *38*(5), 283–290. https://doi.org/10.1175/1520-0477-38.5.283

Bonner, W. D. (1968). Climatology of the low level jet. *Monthly Weather Review*, *96*(12), 833–850. https://doi.org/10.1175/1520-0493(1968)096<0833:COTLLJ>2.0.CO;2

Chen, G. T. J., Wang, C. C., & Lin, D. T. W. (2005). Characteristics of low-level jets over northern Taiwan in mei-yu season and their relationship to heavy rain events. *Monthly Weather Review*, *133*(1), 20–43. https://doi.org/10.1175/MWR-2813.1

Chen, Y. L., Chen, X. A., & Zhang, Y. X. (1994). A diagnostic study of the low-level jet during TAMEX IOP 5. *Monthly Weather Review*, *122*(10), 2257–2284. https://doi.org/10.1175/1520-0493(1994)122<2257:ADSOTL>2.0.CO;2

CMA. (2023). Surface and upper-air observations in China [Dataset]. *China Meteorological Administration*. Retrieved from http://data.cma.cn

Cui, C., Zhou, W., Yang, H., Wang, X., Deng, Y., Wang, X., et al. (2023). Analysis of the characteristics of the low-level jets in the middle reaches of the Yangtze River during the Mei-yu season. *Advances in Atmospheric Sciences*, *40*(4), 711–724. https://doi.org/10.1007/s00376-022-2107-1

Cui, W., Dong, X., Xi, B., & Liu, M. (2020). Cloud and precipitation properties of MCSs along the Meiyu frontal zone in central and southern China and their associated large-scale environments. *Journal of Geophysical Research: Atmospheres*, *125*(6), e2019JD031601. https://doi.org/10.1029/2019JD031601

Du, Y., & Chen, G. (2019). Climatology of low-level jets and their impact on rainfall over southern China during the early-summer rainy season. *Journal of Climate*, *32*(24), 8813–8833. https://doi.org/10.1175/JCLI-D-19-0306.1

Du, Y., & Rotunno, R. (2014). A simple analytical model of the nocturnal low-level jet over the Great Plains of the United States. *Journal of the Atmospheric Sciences*, *71*(10), 3674–3683. https://doi.org/10.1175/JAS-D-14-0060.1

Du, Y., Shen, Y., & Chen, G. (2022). Influence of coastal marine boundary layer jets on rainfall in South China. *Advances in Atmospheric Sciences*, *39*(5), 782–801. https://doi.org/10.1007/s00376-021-1195-7

Du, Y., & Yi, S. (2025). The relationship scenarios between boundary layer jet and coastal heavy rainfall during the pre-summer rainy season of South China. *Journal of Meteorological Research*, *39*(1), 26–40. https://doi.org/10.1007/s13351-025-4138-x

Du, Y., Zhang, Q., Chen, Y. L., Zhao, Y., & Wang, X. (2014). Numerical simulations of spatial distributions and diurnal variations of low-level jets in China during early summer. *Journal of Climate*, *27*(15), 5747–5767. https://doi.org/10.1175/JCLI-D-13-00571.1

Du, Y., Zhang, Q., Ying, Y., & Yang, Y. (2012). Characteristics of low-level jets in Shanghai during the 2008–2009 warm seasons as inferred from wind profiler radar data. *Journal of the Meteorological Society of Japan. Series II*, *90*(6), 891–903. https://doi.org/10.2151/jmsj.2012-603

Farquharson, J. S. (1939). The diurnal variation of wind over tropical Africa. *Quarterly Journal of the Royal Meteorological Society*, *65*(280), 165–184. https://doi.org/10.1002/qj.49706528004

Findlater, J. (1977). Observational aspects of the low-level cross-equatorial jet stream of the western Indian Ocean. *Pure and Applied Geophysics*, *115*(5), 1251–1262. https://doi.org/10.1007/bf00874408

Fu, S. M., Tang, H., Sun, J. H., Zhao, T. B., & Li, W. L. (2022). Historical rankings and vortices' activities of the extreme Mei-yu seasons: Contrast 2020 to previous Mei-yu seasons. *Geophysical Research Letters*, *49*(2), e2021GL096590. https://doi.org/10.1029/2021GL096590

Hersbach, H., Bell, B., Berrisford, P., Hirahara, S., Horányi, A., Muñoz-Sabater, J., et al. (2020). The ERA5 global reanalysis [Dataset]. *Quarterly Journal of the Royal Meteorological Society*, *146*(730), 1999–2049. https://doi.org/10.1002/qj.3803

Holton, J. R. (1967). The diurnal boundary layer wind oscillation above sloping terrain. *Tellus*, *19*(2), 200–205. https://doi.org/10.1111/j.2153-3490.1967.tb01473.x

Hu, Y., Deng, Y., Lin, Y., Zhou, Z., Cui, C., & Dong, X. (2021). Dynamics of the spatiotemporal morphology of Mei-yu fronts: An initial survey. *Climate Dynamics*, *56*(9), 2715–2728. https://doi.org/10.1007/s00382-020-05619-2

Hu, Y., Deng, Y., Lin, Y., Zhou, Z., Cui, C., Li, C., & Dong, X. (2022). Indirect effect of diabatic heating on Mei-yu frontogenesis. *Climate Dynamics*, *59*(3), 851–868. https://doi.org/10.1007/s00382-022-06159-7

Lanzante, J. R. (1996). Resistant, robust and non-parametric techniques for the analysis of climate data: Theory and examples, including applications to historical radiosonde station data. *International Journal of Climatology: A Journal of the Royal Meteorological Society*, *16*(11), 1197–1226. https://doi.org/10.1002/(SICI)1097-0088(199611)16:11<1197::AID-JOC89>3.0.CO;2-L

Li, N., Guo, J., Wu, M., Zhang, F., Guo, X., Sun, Y., et al. (2024). Low-level jet and its effect on the onset of summertime nocturnal rainfall in Beijing. *Geophysical Research Letters*, *51*(20), e2024GL110840. https://doi.org/10.1029/2024GL110840

Lima, D. C., Soares, P. M., Nogueira, M., & Semedo, A. (2022). Global coastal low-level wind jets revisited through the new ERA5 reanalysis. *International Journal of Climatology*, *42*(9), 4491–4507. https://doi.org/10.1002/joc.7482

Liu, H., He, M., Wang, B., & Zhang, Q. (2014). Advances in low-level jet research and future prospects. *Journal of Meteorological Research*, *28*(1), 57–75. https://doi.org/10.1007/s13351-014-3166-8

Liu, S., & Liang, X. Z. (2010). Observed diurnal cycle climatology of planetary boundary layer height. *Journal of Climate*, *23*(21), 5790–5809. https://doi.org/10.1175/2010JCLI3552.1

Liu, X., Luo, Y., Huang, L., Zhang, D. L., & Guan, Z. (2020). Roles of double low-level jets in the generation of coexisting inland and coastal heavy rainfall over south China during the presummer rainy season. *Journal of Geophysical Research: Atmospheres*, *125*(18), e2020JD032890. https://doi.org/10.1029/2020JD032890

Marengo, J. A., Soares, W. R., Saulo, C., & Nicolini, M. (2004). Climatology of the low-level jet east of the Andes as derived from the NCEP–NCAR reanalyses: Characteristics and temporal variability. *Journal of Climate*, *17*(12), 2261–2280. https://doi.org/10.1175/1520-0442(2004)017<2261:COTLJE>2.0.CO;2

Means, L. L. (1952). On thunderstorm forecasting in the central United States. *Monthly Weather Review*, *80*(10), 165–189. https://doi.org/10.1175/1520-0493(1952)080<0165:OTFITC>2.0.CO;2

Miao, Y., Guo, J., Liu, S., Wei, W., Zhang, G., Lin, Y., & Zhai, P. (2018). The climatology of low-level jet in Beijing and Guangzhou, China. *Journal of Geophysical Research: Atmospheres*, *123*(5), 2816–2830. https://doi.org/10.1002/2017JD027321

Montini, T. L., Jones, C., & Carvalho, L. M. (2019). The South American low-level jet: A new climatology, variability, and changes. *Journal of Geophysical Research: Atmospheres*, *124*(3), 1200–1218. https://doi.org/10.1029/2018JD029634

21698996, 2026, 18, Downloaded from https://agupubs.onlinelibrary.wiley.com/doi/10.1029/2026JD047362, Wiley Online Library on [04/11/2026]. See the Terms and Conditions (https://onlinelibrary.wiley.com/terms-and-conditions) on Wiley Online Library for rules of use; OA articles are governed by the applicable Creative Commons License

NOAA National Centers for Environmental Information. (2022). ETOPO 2022 15 arc-second global relief model [Dataset]. *NOAA National Centers for Environmental Information*. https://doi.org/10.25921/fd45-gt74

Pham, N. T., Nakamura, K., Furuzawa, F. A., & Satoh, S. (2008). Characteristics of low level jets over Okinawa in the Baiu and post-Baiu seasons revealed by wind profiler observations. *Journal of the Meteorological Society of Japan. Series II*, *86*(5), 699–717. https://doi.org/10.2151/jmsj.86.699

Rotach, M. W., & Zardi, D. (2007). On the boundary-layer structure over highly complex terrain: Key findings from MAP. *Quarterly Journal of the Royal Meteorological Society: A Journal of the Atmospheric Sciences, Applied Meteorology and Physical Oceanography*, *133*(625), 937–948. https://doi.org/10.1002/qj.71

Shapiro, A., Fedorovich, E., & Rahimi, S. (2016). A unified theory for the Great Plains nocturnal low-level jet. *Journal of the Atmospheric Sciences*, *73*(8), 3037–3057. https://doi.org/10.1175/JAS-D-15-0307.1

Shen, Y., & Du, Y. (2023). Sensitivity of boundary layer parameterization schemes in a marine boundary layer jet and associated precipitation during a coastal warm-sector heavy rainfall event. *Frontiers in Earth Science*, *10*, 1085136. https://doi.org/10.3389/feart.2022.1085136

Shu, H., Zhang, F., Du, Y., Wang, Y., Guo, H., Song, Z., & Zhang, Q. (2024). Characteristics and formation mechanisms of low-level jets in northeastern China. *Advances in Atmospheric Sciences*, *41*(12), 2432–2445. https://doi.org/10.1007/s00376-024-3209-8

Stull, R. (1988). *An introduction to boundary layer meteorology*. Kluwer Academic Publishers. https://doi.org/10.1007/978-94-009-3027-8

Tan, Y., Xin, J., Qin, X., Ma, Y., Xu, J., Du, Y., et al. (2025). Differences among thermal, dynamic, and material boundary layers over complex terrain. *Journal of Geophysical Research: Atmospheres*, *130*(9), e2024JD043043. https://doi.org/10.1029/2024JD043043

Vanderwende, B. J., Lundquist, J. K., Rhodes, M. E., Takle, E. S., & Irvin, S. L. (2015). Observing and simulating the summertime low-level jet in central Iowa. *Monthly Weather Review*, *143*(6), 2319–2336. https://doi.org/10.1175/MWR-D-14-00325.1

Wang, J. F., Yu, F., Ren, Q., & Wei, C. J. (2020). Spatial and temporal variability of turbulent mixing in the near-field of the Changjiang River. *Journal of Oceanology and Limnology*, *38*(4), 1138–1152. https://doi.org/10.1007/s00343-020-0008-7

Wei, Q., Sun, J., Fu, S., Zhang, Y., & Wang, X. (2024). Spatiotemporal characteristics of rainfall over different terrain features in the middle reaches of the Yangtze River Basin during the warm seasons of 2016–20. *Advances in Atmospheric Sciences*, *41*(5), 915–936. https://doi.org/10.1007/s00376-023-3034-5

Wei, W., Wu, B. G., Ye, X. X., Wang, H. X., & Zhang, H. S. (2013). Characteristics and mechanisms of low-level jets in the Yangtze River Delta of China. *Boundary-Layer Meteorology*, *149*(3), 403–424. https://doi.org/10.1007/s10546-013-9852-8

Wei, W., Zhang, H. S., & Ye, X. X. (2014). Comparison of low-level jets along the north coast of China in summer. *Journal of Geophysical Research: Atmospheres*, *119*(16), 9692–9706. https://doi.org/10.1002/2014JD021476

Whiteman, C. D., Bian, X., & Zhong, S. (1997). Low-level jet climatology from enhanced rawinsonde observations at a site in the southern Great Plains. *Journal of Applied Meteorology*, *36*(10), 1363–1376. https://doi.org/10.1175/1520-0450(1997)036<1363:LLJCFE>2.0.CO;2

Xue, M., Luo, X., Zhu, K., Sun, Z., & Fei, J. (2018). The controlling role of boundary layer inertial oscillations in Meiyu frontal precipitation and its diurnal cycles over China. *Journal of Geophysical Research: Atmospheres*, *123*(10), 5090–5115. https://doi.org/10.1029/2018JD028368

Yan, Y., Cai, X., Wang, X., Miao, Y., & Song, Y. (2021). Low-level jet climatology of China derived from long-term radiosonde observations. *Journal of Geophysical Research: Atmospheres*, *126*(20), e2021JD035323. https://doi.org/10.1029/2021JD035323

Yanai, M., Esbensen, S., & Chu, J. H. (1973). Determination of bulk properties of tropical cloud clusters from large-scale heat and moisture budgets. *Journal of the Atmospheric Sciences*, *30*(4), 611–627. https://doi.org/10.1175/1520-0469(1973)030<0611:DOBPOT>2.0.CO;2

Zeng, W., Chen, G., Du, Y., & Wen, Z. (2019). Diurnal variations of low-level winds and precipitation response to large-scale circulations during a heavy rainfall event. *Monthly Weather Review*, *147*(11), 3981–4004. https://doi.org/10.1175/MWR-D-19-0131.1

Zhang, M., & Meng, Z. (2019). Warm-sector heavy rainfall in southern China and its WRF simulation evaluation: A low-level-jet perspective. *Monthly Weather Review*, *147*(12), 4461–4480. https://doi.org/10.1175/MWR-D-19-0110.1

Zhang, Q. H., Lau, K. H., Kuo, Y. H., & Chen, S. J. (2003). A numerical study of a mesoscale convective system over the Taiwan Strait. *Monthly Weather Review*, *131*(6), 1150–1170. https://doi.org/10.1175/1520-0493(2003)131<1150:ANSOAM>2.0.CO;2

Zhang, X., Luo, Y., & Du, Y. (2024). Observation of boundary-layer jets in the northern South China Sea by a research vessel. *Remote Sensing*, *16*(20), 3872. https://doi.org/10.3390/rs16203872

Zhang, Y. C., Fu, S. M., Sun, J. H., Fu, R., Jin, S. L., & Ji, D. S. (2019). A 14-year statistics-based semi-idealized modeling study on the formation of a type of heavy rain–producing southwest vortex. *Atmospheric Science Letters*, *20*(5), e894. https://doi.org/10.1002/asl.894

Zheng, E., Du, Y., Luo, Y., Zhang, Q., Chen, G., Su, L., & Kong, H. (2026). Two types of low-level jets in China during the warm season: Observational climatology from radiosonde data. *Atmospheric and Oceanic Science Letters*, 100791. https://doi.org/10.1016/j.aosl.2026.100791

Zhou, C., Chen, G., Du, Y., & Su, L. (2026). Double low-level jets over South China in the warm season: Diversity and impacts. *Journal of Geophysical Research: Atmospheres*, *131*(7), e2025JD045497. https://doi.org/10.1029/2025JD045497

Zhou, L. A., Wang, C., Miao, S., & Li, J. (2024). Impact of the complex terrain in Beijing on formation of low-level jets. *Journal of Meteorological Research*, *38*(1), 138–150. https://doi.org/10.1007/s13351-024-3122-1

21698996, 2026, 18, Downloaded from https://agupubs.onlinelibrary.wiley.com/doi/10.1029/2026JD047362, Wiley Online Library on [04/11/2026]. See the Terms and Conditions (https://onlinelibrary.wiley.com/terms-and-conditions) on Wiley Online Library for rules of use; OA articles are governed by the applicable Creative Commons License